Planar array magnetic induction tomography further improvement

F Li[1], JFPJ Abascal[2], M Soleimani[1]

[1]*Engineering Tomography Lab (ETL), Electronic and Electrical Engineering, University of Bath, Bath, UK*
[2]*Univ Lyon, INSA - Lyon, Université Claude Bernard Lyon 1, UJM-Saint Etienne, CNRS, Inserm, CREATIS UMR 5220, U1206, Lyon, France*

Abstract

Purpose – Magnetic induction tomography (MIT) is a tomographic imaging technique with a wide range of potential industrial applications. Planar array MIT is a convenient set-up but unable to access freely from the entire periphery as it only collects measurements from one surface, so it remains very challenging given the limited data. This study assesses the use of sparse regularization methods for accurate position and depth detection in planar array MIT.

Design/methodology/approach – The most difficult challenges in MIT are to solve the inverse and forward problems. The inversion of planar MIT is severely ill-posed due to limited access data. Thus, this paper posed a total variation problem and solved it efficiently with the Split Bregman formulation to overcome this difficulty. Both isotropic and anisotropic total variation formulations are compared to Tikhonov regularization with experimental MIT data.

Findings – Results show that Tikhonov method failed or underestimated the object position and depth. Both isotropic and anisotropic total variation led to accurate recovery of depth and position.

Originality/value – There are numerous potential applications for planar array MIT where access to the materials under testing is restrict. Sparse regularization methods are a promising approach to improving depth detection for limited MIT data.

Keywords Magnetic induction tomography, Total variation, Planar array MIT system, Isotropic TV, Anisotropic TV

Paper type Research paper

1. Introduction

Magnetic induction tomography (MIT) is a non-destructive and widely used tomographic imaging technique that can map the electromagnetic properties of an object based on eddy current theories. In theory, MIT is capable of imaging all three passive electromagnetic properties (PEP), i.e., permittivity, permeability and conductivity but it generally aims at reconstructing the conductivity distribution of the test samples. In recent years, MIT was developed for both medical and industrial applications such as stroke detection (Park and Kim, 2005), molten metal flow monitoring (Ma et al., 2005), non-destructive testing (NDT) for material characterization (Wei and Soleimani, 2012) and as a potential detection tool for National Nuclear Security ((Darrer et al., 2015))

MIT is aiming at visualizing the conductivity distribution of the test sample, which can be achieved by solving the forward and inverse problem. The forward problem can be easily

elucidated by eddy current model while regularization is required to solve the inverse problem due to its ill-posed nature. Tikhonov regularization is the tradition and most widely used regularization method in MIT system but leads to suboptimal results. A better choice is to use total variation (TV) functional that can improve the reconstructed image quality over Tikhonov regularization. Total variation allows to regularize the inverse problem by removing noise while preserving edges in the reconstructed images. However, TV functional is non-differentiable, so it is usually approximated. These approximations may be non-optimal or lead to slow convergence. In addition, TV may lead to a loss of contrast (Burger et al., 2013). The use of the Bregman distance has been proposed to solve these issues (Burger et al., 2013). In particular, the split Bregman method solves efficiently L1-regularized problems such as the total variation and has been widely applied to different applications (Osher et al., 2005, Wang et al., 2012, Abascal et al., 2011, Goldstein and Osher, 2009, Abascal et al., 2016). A recent study (Li et al., 2017) proposed the use of TV functional to improve the reconstructed image quality over Tikhonov regularization on MIT experimental data.

The TV problem first proposed in (Rudin et al., 1992) for noise removal was based on the isotropic formulation of TV. Anisotropic TV has been suggested in different applications (Chen et al., 2013, Werlberger et al., 2009). Anisotropic diffusion regularization was investigated in (Correia et al., 2011) for fluorescence diffuse optical tomography. For efficient noise removal, isotropic and anisotropic TV can outperform each other depending on the application. Isotropic TV prefers boundaries that have not preferred orientation in space and weights equally the contributions in all directions while anisotropic TV preserves edges that are aligned along the coordinates axes (Esedoğlu and Osher, 2004, Lou et al., 2015). In the case of planar imaging MIT there is a decrease of resolution with depth, so the depth direction should be treated independently. In this paper, Isotropic TV and Anisotropic TV are implemented in planar sensor array MIT for position detection and depth detection.

MIT can be divided into different types of systems based on its spatial arrangements of coils, i.e., traditional circular array MIT and planar array MIT (Figure 1). The measured region of traditional circular array MIT system can access freely around the entire periphery. As such, many previous researches indicate the capability of circular array MIT system where the object space has circular geometry and free access. However, there are plenty of situations where the access is so restricted that non-destructive measurements cannot be collected from the complete periphery but only from one surface(Ramli and Peyton, 1999). The test space of the system proposed in this paper is perpendicular to the sensors in order to overcome these difficulties and the resulting application of this technique has increased considerably. Since that, a series of studies based on planar system have been recently implemented. The feasibility of planar type coil used for evaluating near-surface material properties was investigated in (Goldfine, 1996). In (Mukhopadhyay et al., 2001), authors investigated the possibility of inspection of electroplated materials using planar meander and mesh type magnetic sensor. The planar MIT system for the detection of faults on thin metallic plates was presented in (Yin and Peyton, 2006), which shows 2D imaging results underneath the sensor array. The work in (Ma et al., 2013) explored the feasibility of planar MIT system for 3D near subsurface imaging through simulation results and experimental evaluations. From the previous observations, planar array MIT system shows significant challenge in terms of depth detection over traditional circular array system. The development and set up of the proposed planar array MIT system are presented in this paper, followed by the experimental results of position and depth detection.

In this work, the capabilities of proposed planar array MIT system with both isotropic and isotropic TV regularization methods for position and depth detection are evaluated by experimental data. Results in this study support that the planar MIT system with the aid of TV regularization would receive considerable attention in subsurface imaging area.

Figure 1 Planar sensor array MIT system

Figure 2 The proposed planar array MIT system

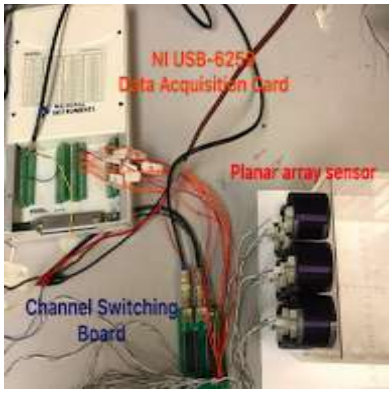

2. Methodology

2.1 Forward problem

MIT forward problem can be elucidated by eddy current problem. The MIT domain can be defined into two regions: non-conducting region Ω_n and eddy current region Ω_e. In this paper, the eddy current problem is solved with the aids of finite element method (FEM) and magnetic vector potential: free space magnetic vector potential A_s and reduced magnetic vector potential A_r(Li et al., 2017, Biro and Preis, 1989, Soleimani et al., 2006, Bíró, 1999). Then the (A^*_r, A_r) formulation can be expressed as following:

$$\nabla \times \frac{1}{\mu} \nabla \times A_r + j\omega\sigma A_r = \nabla \times H_s - \nabla \times \frac{1}{\mu}(\mu_0 H_s) - jw\sigma A_s \quad (1)$$

where μ is magnetic permeability, μ_0 is free space magnetic permeability, ω is angular frequency, σ is electrical conductivity and H_s is the magnetic field density in free space.

In the case of $\mu_0 = \mu$, after transforming the previous equation and applying Galerkin's formulation, the Galerkin's approximation can be obtained:

$$\int_\Omega \left(\nabla \times \boldsymbol{N}_i \cdot \frac{1}{\mu} \nabla \times A_r\right) dv + \int_{\Omega_e} (j\omega\sigma \boldsymbol{N}_i \cdot A_r) dv = -\int_{\Omega_e} ((j\omega\sigma \boldsymbol{N}_i \cdot A_s) dv - \int_{\Omega_n} (\nabla \times \boldsymbol{N}_i \cdot H_s) dv \quad (2)$$

where $\boldsymbol{N}_i$ is the linear combination of edge shape functions, $\Omega = \Omega_{e+}\Omega_{n+}\Omega_Q$ entire modelling domain, Ω_e and Ω_n are eddy current region and excitation coil region (Ω_Q current source region within non-conductive region) respectively. The right hand side of equation (2) can be solved with the aid of Biot-Savart theory. And if J_0 is the unit current density passing through coil and $A = A_r + A_s$, the measured induced voltage in sensing coil can be calculated as following:

$$V_{mn} = -\left(\frac{j\omega}{S^{(m)}}\right) \int_{(\Omega_Q)} (A^{(n)} \cdot j_0^{(m)}) \, dv \quad (3)$$

where $j_0^{(m)} = J_0^{(m)} / \left|J_0^{(m)}\right|$ and $S^{(m)}$ is the cross-section area of the mth-coil.

If I is the total current passing through the excitation coil, the Jacobian matrix can be expressed by

$$J_{mn} = \frac{\partial V_{mn}}{\partial \sigma_x} = -\omega^2 \frac{\int_{\Omega_x} A_m \cdot A_n dv}{I} \quad (4)$$

where A_m is the forward solver of excitation coil m excited with I, A_n is the forward solver of sensor coil excited by unit current, σ_x is the conductivity of voxel x and Ω_x is the volume of the perturbation(Lionheart et al, 2003).

2.2 Inverse problem

It is common practice to adopt dynamic imaging for reconstructing experimental data, as it less sensitive to modelling errors. Let F be the forward operator that provides boundary voltage v given a conductivity distribution σ, i.e. $v = F(\sigma)$. In dynamic imaging, boundary voltages without object, $v_0 = F(\sigma_0)$, are available, so a linear inverse problem is defined as the recovery of a change in conductivity $\Delta\sigma$ from a change in boundary voltage Δv, where $J\Delta\sigma = \Delta v$ and J is the Jacobian or sensitivity matrix.

- **Tikhonov regularization method**

The Tikhonov regularization method, which has been widely used in experimental MIT, is used as a comparison. Let $\Delta\sigma_\alpha$ be the optimal solution of inverse problem, $\Delta\sigma_0$ an initial estimate image and Δv the measurements. The Tikhonov regularization method can be expressed as following (Merwa et al., 2005):

$$\Delta\sigma_\alpha = argmin_{\Delta\sigma}(\|J\Delta\sigma - \Delta v\|^2 + \gamma^2\|R\,(\Delta\sigma - \Delta\sigma_0)\|^2) \quad (5)$$

where R is a regularization matrix, γ is the regularization parameter.

- **Isotropic and anisotropic total variation methods**

The total variation method aims to solve the following constrained optimization problem

$$\Delta\sigma = argmin_{\Delta\sigma}\|\nabla\Delta\sigma\|_1 \; such\; that \; \|J\Delta\sigma - \Delta v\|^2 \le \rho \quad (6)$$

where ρ accounts for noisy data, $\|\nabla\,\Delta\sigma\|_1$ is the total variation functional, ∇ the spatial gradient and $\|\cdot\|_1$ the $l_1 - norm$. The isotropic version of the discrete TV functional (Goldstein and Osher, 2009) is usually adopted:

$$\|\nabla\,\Delta\sigma\|_1 = \sum_{i=1}^{n}\sqrt{(\nabla_x\Delta\sigma)_i^2 + \left(\nabla_y\Delta\sigma\right)_i^2 + (\nabla_z\Delta\sigma)_i^2} \quad (7)$$

where n is the number of pixels in the image. The anisotropic form of TV allows to separate and to weight the contributions along the diffe rent directions:

$$\|\nabla\,\Delta\sigma\|_1 = \alpha_x\|\nabla_x\,\Delta\sigma\|_1 + \alpha_y\left\|\nabla_y\,\Delta\sigma\right\|_1 + \alpha_z\|\nabla_z\,\Delta\sigma\|_1 \quad (8)$$

- **Resolution with the split Bregman method**

The constrained problem (6) can be solved using standard optimization approaches, but these can be computationally expensive and difficult to implement. A simpler and more efficient approach is to build a regularization scheme based on the use of the Bregman distance, which leads to a sequence of unconstrained problems whose solution converge to the solution of the constrained problem (6) (Osher et al., 2005). For a given convex functional $C\,(x)$, the Bregman distance between x and y is defined as

$$D_C\,(x,y) = C\,(x) - C\,(y) - < s, x - y > \quad (9)$$

where s is the subgradient of C at y, and $<,>$ denotes the scalar product. In this work, $C\,(x)$ is the total variation function defined in equations (7) or (8). Then, the Bregman iterative algorithm can be expressed as the following iterative procedure:

$$\Delta\sigma^{k+1} = argmin_{\Delta\sigma}\, D_C\left(\Delta\sigma, \Delta\sigma^k\right) + \frac{\mu}{2}\|J\Delta\sigma - \Delta v\|^2 \quad (10)$$

$$s^{k+1} = s^k - \mu J^T(J\Delta\sigma^{k+1} - \Delta v) \quad (11)$$

where $D_C\left(\Delta\sigma, \Delta\sigma^k\right)$ is the Bregman distance between the optimal solution $\Delta\sigma$ and the solution at the previous step $\Delta\sigma^k$, and s^{k+1} is the sub gradient of the total variation function at the $(k+1)\,th$-iteration.

For linear operators *J,* the iterative scheme (10-11) can be simplified as following

$$\Delta\sigma^{k+1} = argmin_{\Delta\sigma}\{\|\nabla\Delta\sigma\|_1 + \frac{\mu}{2}\left\|J\Delta\sigma - (\Delta v)^k\right\|^2\} \quad (12)$$

$$\Delta v^{k+1} = \Delta v^k + \Delta v - J\Delta\sigma^{k+1} \quad (13)$$

where (13) is the Bregman iteration that impo ses the constraint iteratively.

Equation (12) can be solved now at every iteration with conventional unconstrained optimization algorithms. However, it is still difficult to solve because of the non-differentiability of the TV functional.

The split Bregman method can extend the utility of the Bregman iteration to minimize the TV functional in an efficient manner (Goldstein and Osher, 2009). Auxiliary variables can be used to convert equation (12) to a constrained optimization problem in which L2- and L1-problems are decoupled and so easier to solve. We develop the solution only for isotropic TV and then give the solution for anisotropic TV.

For isotropic TV, problem (12) becomes

$$(\Delta\sigma^{k+1}, d_i^{k+1}) = argmin_{\Delta\sigma,d_i}\frac{\mu}{2}\left\|J\Delta\sigma - \Delta v^k\right\|^2 + \left\|\left(d_x, d_y, d_z\right)\right\|_1 \; such\; that \; d_i = \nabla_i\,\Delta\sigma \quad (14)$$

where *i=x,y,z*. To solve this constrained problem, after applying the Bregman iteration as above, the equation (14) can be written as

$$(\Delta\sigma^{k+1}, d_i^{k+1}) = argmin_{\Delta\sigma,d_i}\frac{\mu}{2}\left\|J\Delta\sigma - \Delta v^k\right\|^2 + \left\|\left(d_x, d_y, d_z\right)\right\|_1 + \sum_i\frac{\lambda}{2}\left\|d_i - \nabla_i\Delta\sigma - b_i^k\right\|^2 \quad (15)$$

$$b_i^{k+1} = b_i^k + \nabla_i\Delta\sigma^{k+1} - d_i^{k+1} \quad (16)$$

Then minimizing equation (15) can be achieved by minimizing $\Delta\sigma$ and d_i separately as following (Abascal et al., 2011):

$$\Delta\sigma^{k+1} = argmin_{\Delta\sigma}\frac{\mu}{2}\left\|J\Delta\sigma - \Delta v^k\right\|^2 + \sum_i\frac{\lambda}{2}\left\|d_i^k -\right.$$

$$\nabla_i \Delta\sigma - b_i^k\|^2 \quad (17)$$

$$d_i^{k+1} = argmin_{d_i}\|(d_x, d_y, d_z)\|_1 + \sum_i \frac{\lambda}{2}\|d_i - \nabla_i \Delta\sigma^{k+1} - b_i^k\|^2 \quad (18)$$

Solutions to $\Delta\sigma^{k+1}$ and d_i^{k+1} are given by analytic expressions that can be efficiently computed. $\Delta\sigma^{k+1}$ is given in terms of a linear system and d_i^{k+1} by a shrinkage formula for isotropic formulation (Goldstein and Osher, 2009). The solution for the isotropic TV problem is given as follows:

$$(\mu J^T J + \lambda \sum_i \nabla_i^T \nabla_i)\Delta\sigma^{k+1} = \mu J^T \Delta v^k + \lambda \sum_i \nabla_i^T (b_i^k - d_i^k) \quad (19)$$

$$d_i^{k+1} = \max\left(p^k - \frac{1}{\lambda}, 0\right)\frac{\nabla_i \Delta\sigma^{k+1} + b_i^k}{p^k} \quad (20)$$

$$p^k = \sqrt{\sum_i |\nabla_i \Delta\sigma^{k+1} + b_i^k|^2} \quad (21)$$

$$b_i^{k+1} = b_i^k + \nabla_i \Delta\sigma^{k+1} - d_i^{k+1} \quad (22)$$

$$\Delta v^{k+1} = \Delta v^k + \Delta v - J\Delta\sigma^{k+1} \quad (23)$$

For anisotropic TV, problem (12) becomes

$$(\Delta\sigma^{k+1}, d_i^{k+1}) = argmin_{\Delta\sigma, d_i} \frac{\mu}{2}\|J\Delta\sigma - \Delta v^k\|^2 + \sum_i \alpha_i \|\nabla_i \Delta\sigma\|_1 \quad such\ that\ \ d_i = \nabla_i \Delta\sigma \quad (24)$$

where *i=x,y,z*. Proceeding as above, the final solution for the anisotropic TV problem gives the same solution for $\Delta\sigma^{k+1}$ but auxiliary variables d_i are now given by a different shrinkage formula:

$$d_i^{k+1} = \max\left(|\nabla_i \Delta\sigma^{k+1} + b_i^k| - \frac{\alpha_i}{\lambda}, 0\right)\frac{\nabla_i \Delta\sigma^{k+1} + b_i^k}{|\nabla_i \Delta\sigma^{k+1} + b_i^k|}$$

The only difference between isotropic and anisotropic formulations are the shrinkage or thresholding operations that impose TV iteratively.

Hence, the split Bregman method provides a sequence of solutions ($\Delta\sigma^{k+1}$,$d_i{}^{k+1}$) that converges to the solution of the constrained optimization problem (6). One of the benefits of the split Bregman formulation is that it does not require explicit calculation of the derivatives of the TV functional, which must be otherwise approximated because of the no differentiability of the TV functional. These approximations used by more standard approaches are generally non-optimal and lead to slow convergence. The imaging parameters are selected empirically but in future we aim to use machine learning for such a parameter selection task.

3. Experimental Results

3.1 Planar array MIT System description

The picture of planar MIT system described in this paper is shown in Figure 2. It consists of the following components, includes: a host computer, a digital function generator (Topward 8112), a National Instrument based data acquisition system (NI USB-6259), a channel switching board (ADG406 multiplexers), and a sensor array containing 9 equally spaced inductive coils.

Figure 3 Coil sequence and dimensions

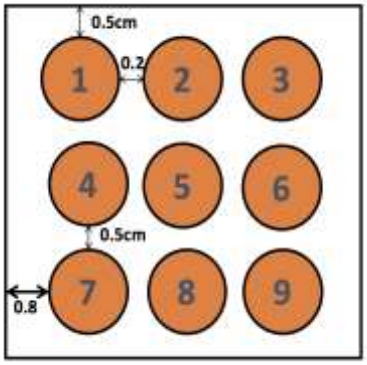

Figure 4 Simplified top view of experimental scenario

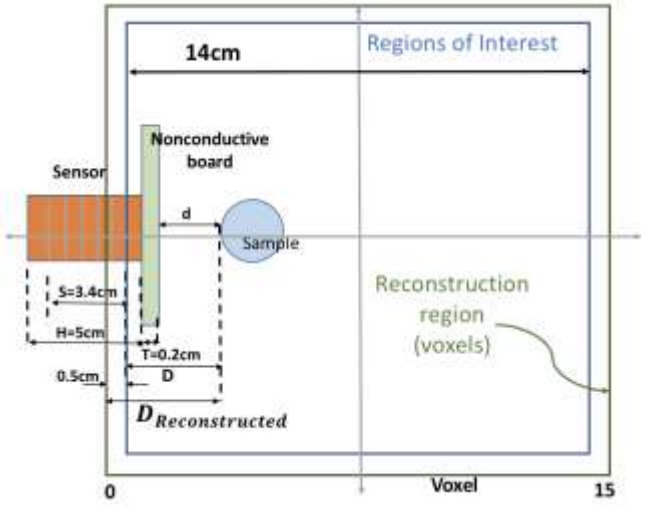

The digital function generator supplies an 80kHz, 15V peak-peak sinusoidal signal to each of the 9 inductive coils individually. The ADG406 multiplexers can accomplish the channel switching process while a NI USB-6259 is connected between a host PC and the multiplexer to do the image reconstruction. All the measurements are averaged three times before displayed. The planar sensor array consists of 9 cylindrical coils, which is

arranged in a 3×3 matrix form and located on a non-conductive square board. The parameters of the sensor model are shown in Table 1. Figure 3 indicates the sequence of the coils. The data collection pattern of this system can be described as the following sequence: 1-2,1-3…1- 9, 2-3…2-8… 8-9 , providing $9 \times 8/2 = 36$ independent measurements that are imported into image reconstruction system.

As it mentioned before, finite element method (FEM) has been applied in this paper. The information of the mesh been used, and the implementation process of the proposed experiments are shown in Figure 5. Moreover, the average total variation reconstruction time is 20 seconds, which is a bit longer than Tikhonov method (2 seconds).

Figure 5 Implementation process of all proposed experiments

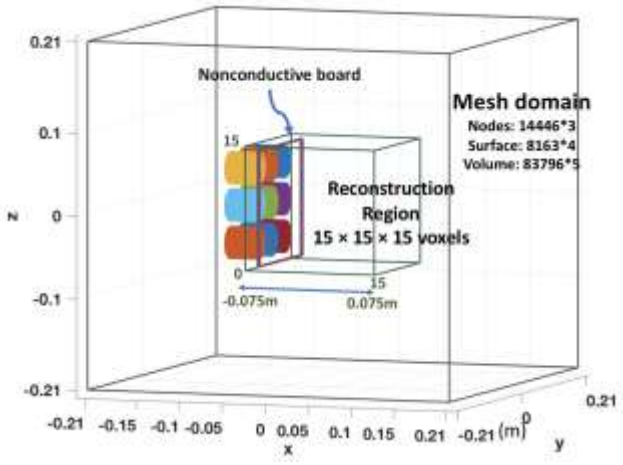

Table 1 Parameters of the sensors model

Number of coils	9
Number of turns	100
Self-inductance (μH)	380
Coil height (cm) (H)	5
Coil side length (cm) (S)	3.4
Outer diameter (cm)	4.1
Inner diameter (cm)	3.9
Surface area of the board (cm^2)	14×14
Thickness of the board (cm) (T)	0.2

All the parameter values were used to solve the inverse problem of the following research are shown in Table 2.

Table 2 Parameter values used to solve the inverse problem

Parameter	Position detection		Depth detection		
	Tikh	Iso	Tikh	Iso	Ani
a1	1e-10		1e-10		
a2	1e3		1e3		
mu		0.2		0.2	0.5
lambda		1e-2		1e-2	1e-3
gamma		1e-1		1e-1	1e-2
thresholding	0.5	0.5	0.5	0.5	0.5

3.2 Position detection using Isotropic TV

In this section, we investigate the capability of planar array MIT system for position detection in terms of a set of experiments. Aluminum rods are used as tested samples and Table 3 shows the parameters of these rods. The aluminum rods are placed in different positions but with the same distance to the sensors, which can be calculated from Figure 4 as $D = T + (H - S)/2 + d$.

Table 3 Parameters of testing rods

Radius of the rods (cm)	2
Height of the rods (cm)	5
Relative permeability	1
Electrical conductivity (S/m)	3.5×10^7
Distance to the sensor (cm)	1

Two sets of experiments are implemented in this section: single and multiple samples. Moreover, isotropic TV and Tikhonov regularization method are used for image reconstruction. The experimental setup for one of the tested configurations is shown in Figure 6; the corresponding simulated image of inclusion indicating the field of view is given in Figure 7.

Figure 6 Experimental setup: sample close to coil1

close to coil1

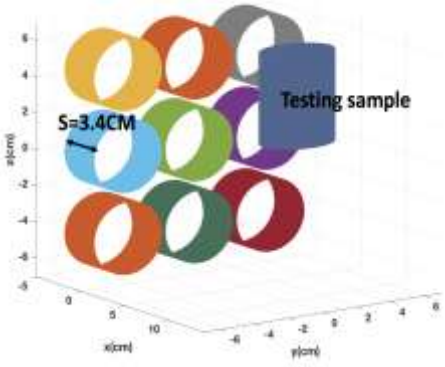

Figure 7 Simulated image of inclusion: sample

Figure 8 indicates the slice images obtained when a single rod is placed in different positions. The images above the sliced images are simulated images of inclusions. Results show that isotropic TV provides exact recovery of positions on tested samples. Figure 9 shows the image results when the tested samples are two aluminum rods. As shown on the sliced images, planar MIT system can also detect multiple samples with much clearer results from isotropic TV method than from Tikhonov regularization.

Figure 8 Position detection of planar MIT using experimental data (single rod) obtained by isotropic TV algorithm

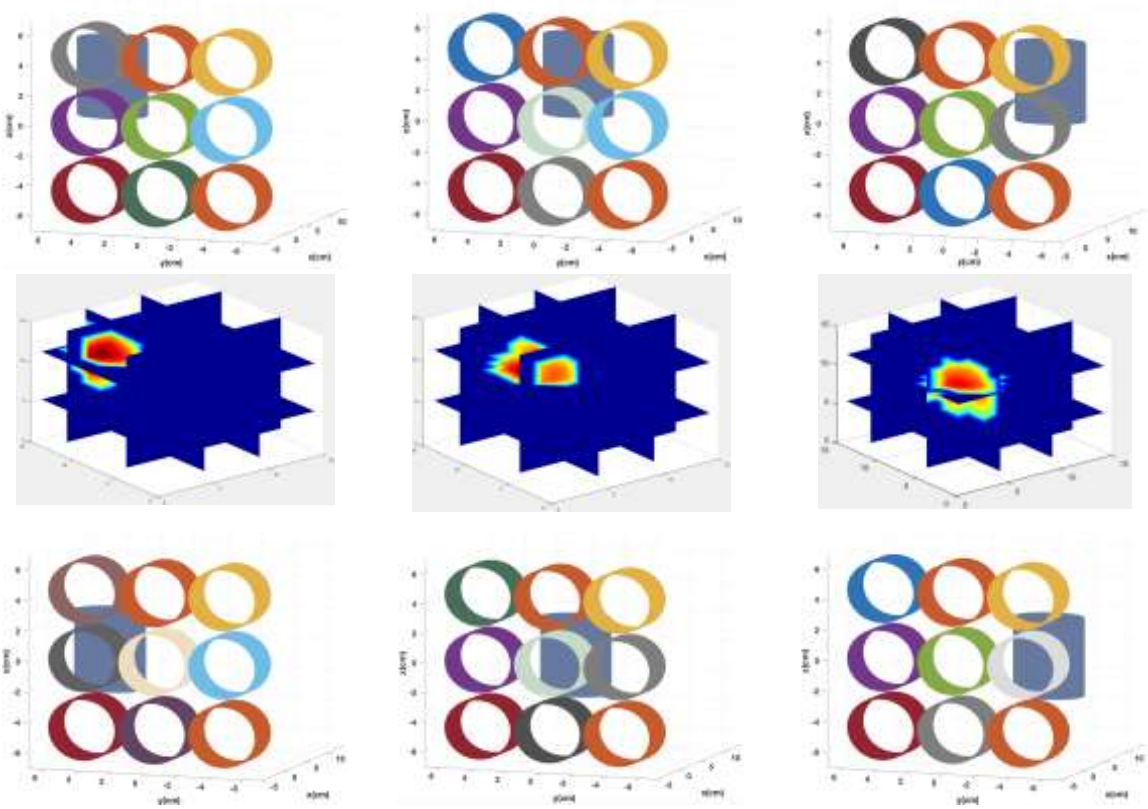

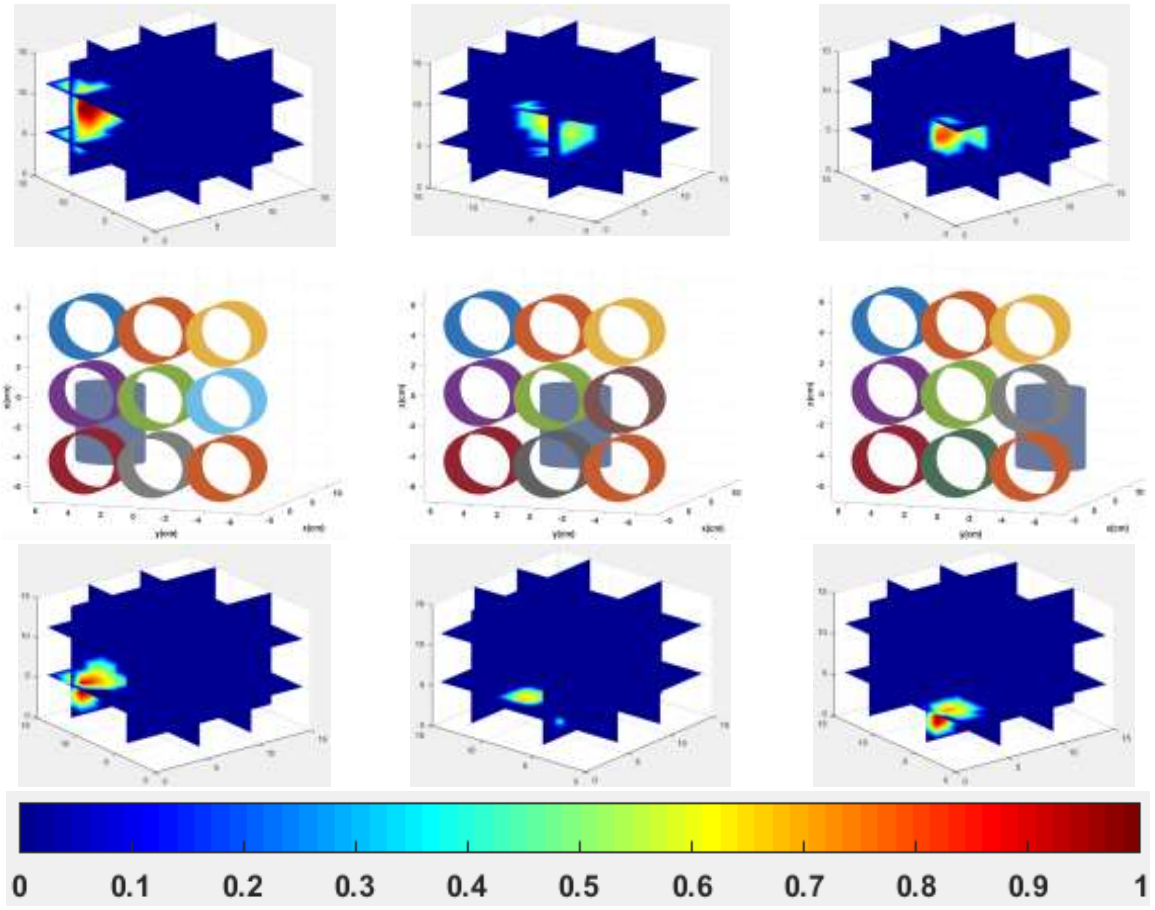

Figure 9 Position detection of planar MIT system using experimental data (multiple rods) obtained by isotropic TV and Tikhonov regularization methods

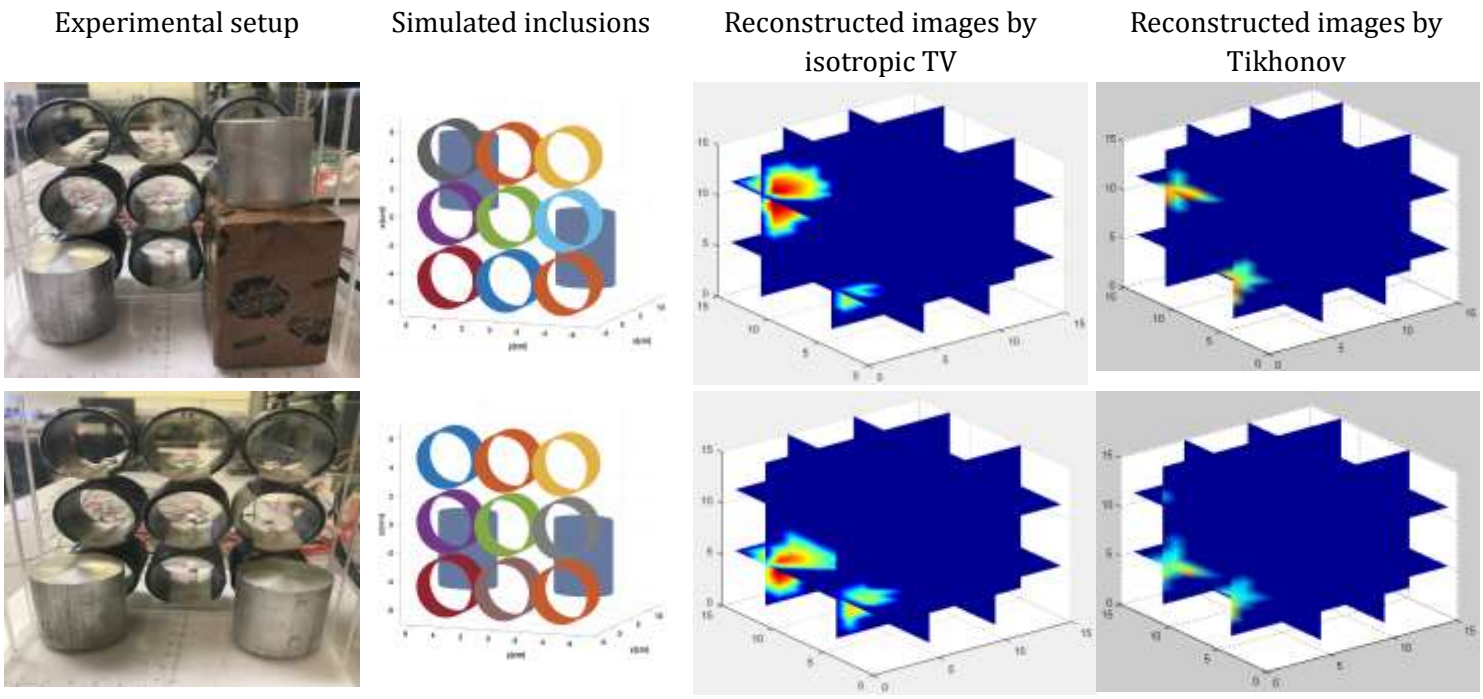

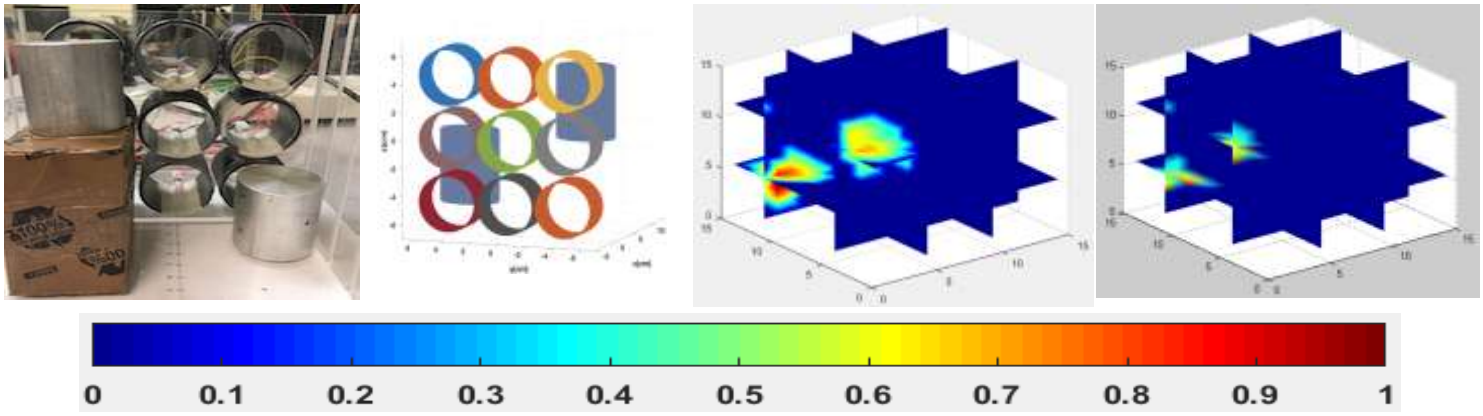

3.3 Depth analysis based on isotropic TV, anisotropic TV and Tikhonov regularization

It has been shown in the previous section that planar array MIT system can detect the objects when they are very close to the sensors. However, to assess the suitability of planar MIT for subsurface imaging we must assess how deep it can detect an object. Therefore, planar MIT with TV regularization is evaluated on different depth detections compared to Tikhonov regularization. The tested sample is the same as the one used in the previous section. The reconstructed images below are obtained by isotropic TV, anisotropic TV and Tikhonov regularization method. An example of experimental setup and simulated image of inclusion are displayed in Figure 10 and 11, respectively.

Figure 10 Experimental setup: D = 1cm

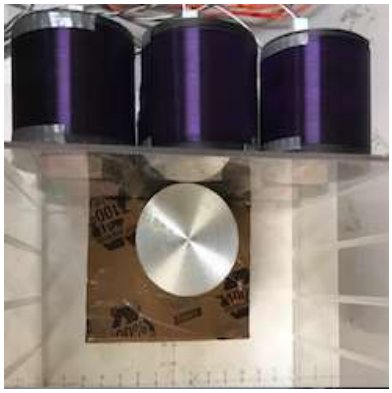

Figure 11 Simulated image of inclusion: D = 1cm

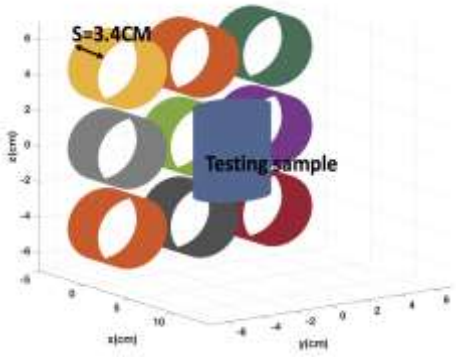

Figure 12 indicates the true experimental setup and reconstructed images using one aluminum rod moving from $D = 1\ cm$ to $D = 5\ cm$. The results include both reconstructed images obtained by isotropic TV, anisotropic TV and Tikhonov regularization methods. All the reconstructed images are the cross-section of identified objects obtained at one slice that is located in the middle of the sensor coils. Results show that TV regularization is sensitive to the depths of sample in accordance with real experimental setup and demonstrate a limit detectability distance of $5\ cm$. On the contrary, the true depth information cannot be extracted from the reconstructed images obtained using Tikhonov regularization. Isotropic and anisotropic TV methods produced similar results, even reconstructed images obtained by anisotropic TV seem slightly better. This might be because a coarse mesh has been used.

Figure 12 Depth detection of planar array MIT system using the experimental data (one rod) obtained by isotropic TV, anisotropic TV and Tikhonov regularization methods

Simulated inclusions	Isotropic TV	Anisotropic TV	Tikhonov regularization
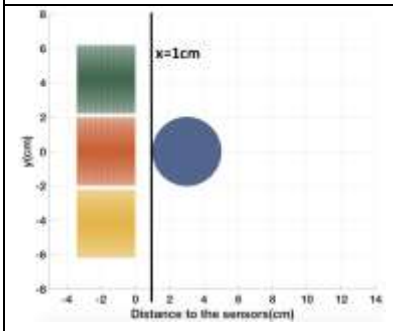	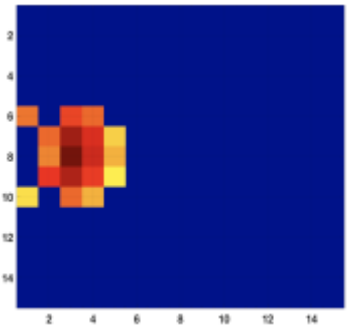 $D_{Reconstructed} = 1.5cm$	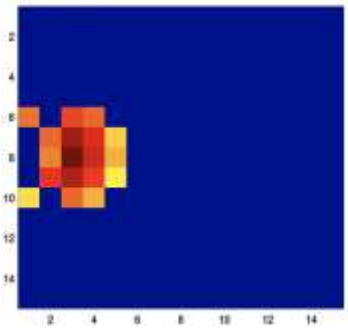 $D_{Reconstructed} = 1.5cm$	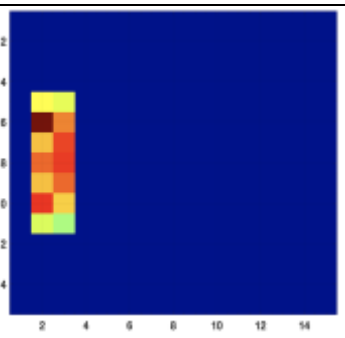 $D_{Reconstructed} = 1.5cm$
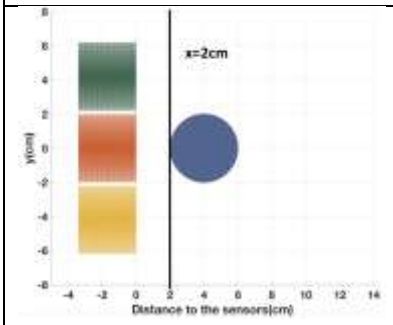	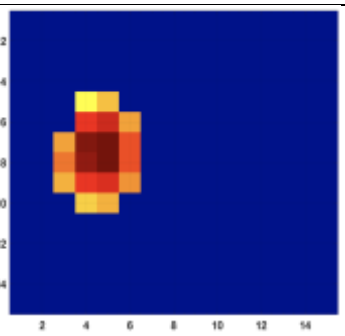 $D_{Reconstructed} = 2.5cm$	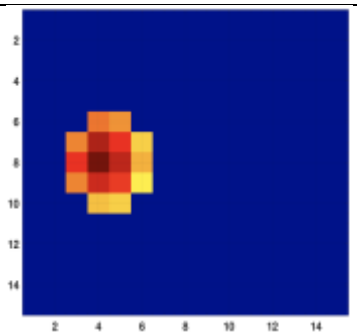 $D_{Reconstructed} = 2.5cm$	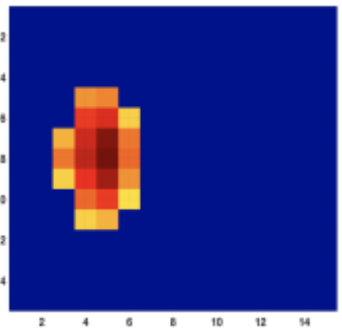 $D_{Reconstructed} = 2.5cm$
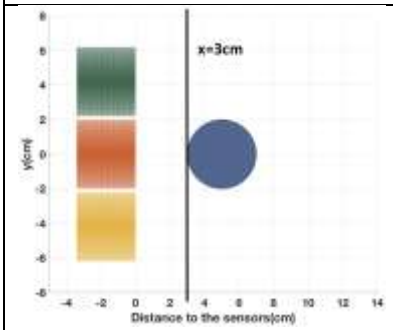	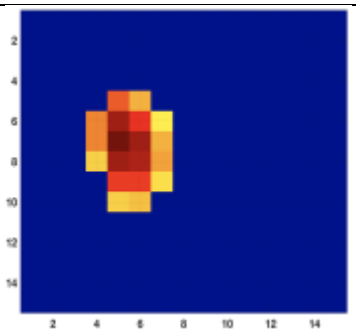 $D_{Reconstructed} = 3.5cm$	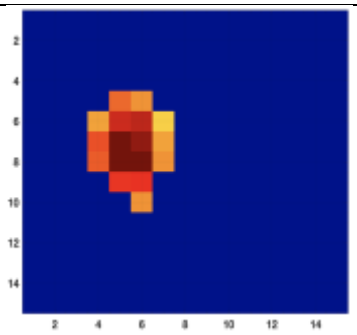 $D_{Reconstructed} = 3.5cm$	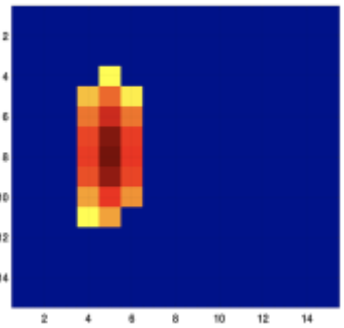 $D_{Reconstructed} = 3.5cm$
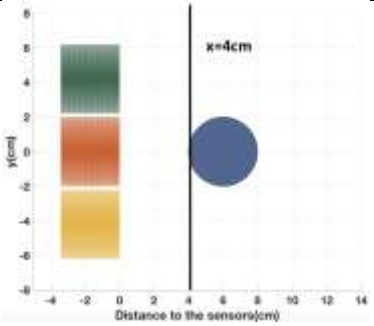	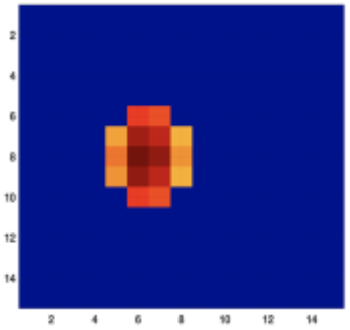 $D_{Reconstructed} = 4.5cm$	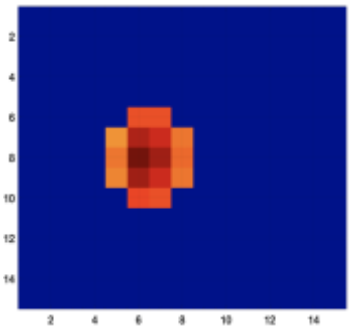 $D_{Reconstructed} = 4.5cm$	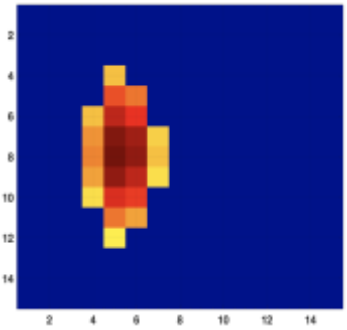 $D_{Reconstructed} = 3.5cm$
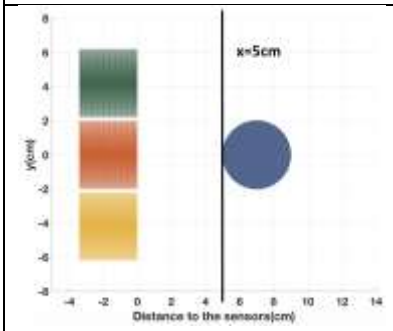	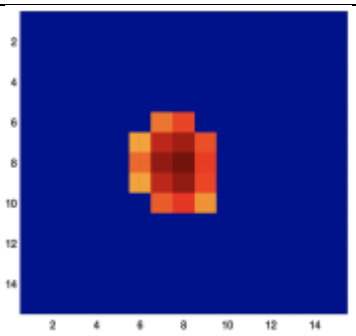 $D_{Reconstructed} = 5.5cm$	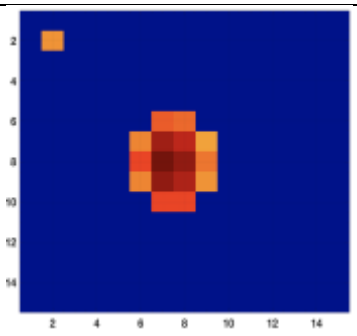 $D_{Reconstructed} = 5.5cm$	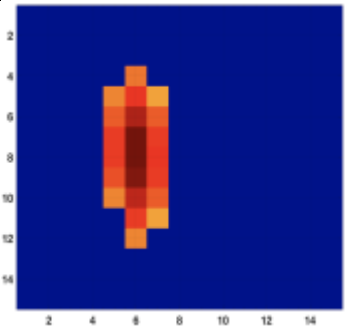 $D_{Reconstructed} = 4.5cm$

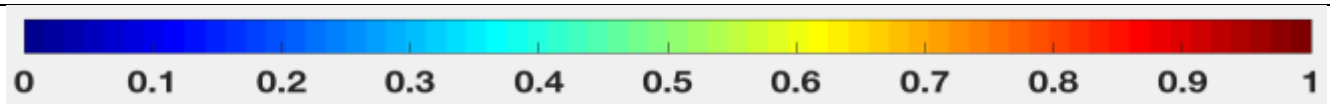

4. Results analysis and discussion

Here we introduced the percentage depth sensitivity (PDS) to indicate the performance of planar MIT system for depth detection:

$$PDS = \frac{(maximum\ detectable\ depth)}{(side\ length\ of\ non-conductive\ square\ board)} \times 100\%$$

The surface area of the square board can be assumed to represent the area of planar array sensors arranged for MIT system. A previous work on planar MIT system (Ma et al., 2013), which introduced a 16-channels planar MIT with a $18 \times 18cm^2$ square board, could detect a maximum depth of $4cm$, and presented PDS that can be estimated as ${}^{4}/_{18} \times 100\% = 22.2\%$. In our experimental study, the maximum depth that could be detected is $5cm$, which corresponds to PDS of ${}^{5}/_{14} \times 100\% = 35.7\%$. This verifies that our framework has a better performance for depth detection than previous methods.

It can be observed from the experimental results in Figure 8&9 that planar array MIT system can detect the positions of single and multiple conductive samples with the aid of total variation regularization algorithm. Figure 12 shows that TV helps to provide more precise images than Tikhonov regularization, enhancing depth detectability of planar MIT. To demonstrate these, three groups of analysis works are conducted below.

The absolute value of the difference between experimental and background induced voltage can be used to determine the sensitivity of the system and so to analyze the depth detection of planar MIT system. Also, this norm of difference is divided by the norm of background data. The system becomes less sensitive as the norm value decreases. Figure 8 shows norm values of 6 experimental measurements conducted in depth detection part. As it shown in Figure 13, a significant decline in norm value of experimental data can be observed. But the norm value will increase when the distance exceeds the limit depth of $5cm$ due to the noises or the less sensitive of system. Obviously, the sensitivity and accuracy of the system degrades as the depth increases.

Figure 13 The norm value of the difference between experimental and background induced voltage

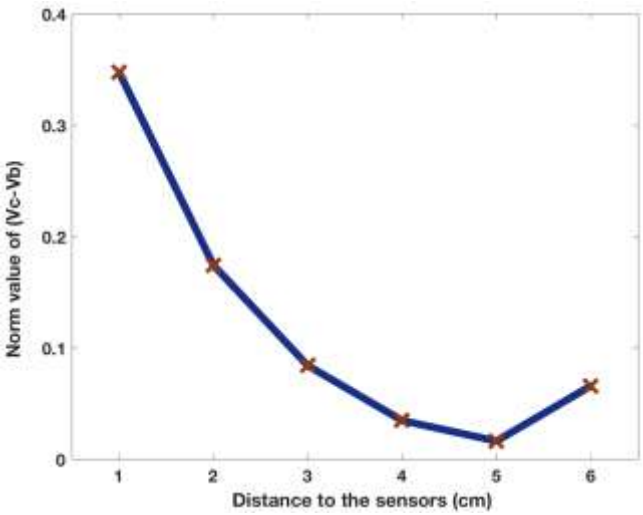

As it can be obtained from results in depth detection, reconstructed images produced by TV regularization have higher image qualities than Tikhonov regularization. Figure 4 demonstrates that the experimental distance can be obtained from the distance shown in reconstructed image as following: $D = D_{Reconstructed} - 0.5$. Then, $D_{Reconstructed}$ can be read from the reconstructed images and the voxel size is $1cm \times 1cm \times 1cm$. Therefore, the distance between the object and the planar sensors can be concisely and explicitly calculated from Figure 11. Figure 14 shows the graph of experimental distances of isotropic TV, anisotropic TV and Tikhonov versus real distances. Moreover, Table 4 explicitly lists the numerical values of experimental distance and the accuracy of depth acknowledged by isotropic TV, anisotropic TV and Tikhonov. Evidentially, the accuracy of the system for depth detection is slightly better with isotropic TV and anisotropic TV than with Tikhonov.

Figure 14 Experimental distance against real distance

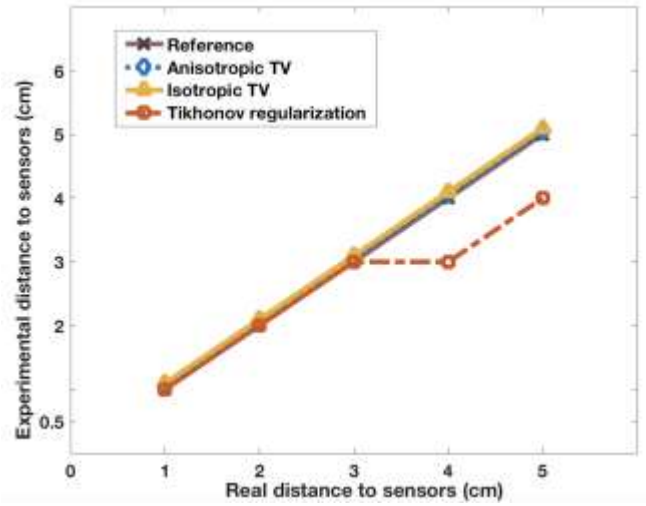

Table 4 The accuracies of depth acknowledged by inverse problem solvers

Reconstructed Distance / Real Distance	Isotropic TV (cm)	Anisotropic TV (cm)	Tikhonov (cm)
1cm	1	1	1
2cm	2	2	2
3cm	3	3	3
4cm	4	4	3
5cm	5	5	4
Average accuracy	100%	100%	91%

Moreover, we present an indicator VR (volume of reconstructed object) to assess the shape of reconstructed objects using planar array MIT system in depth detection. As mentioned before, reconstructed images displayed in this paper are all obtained by applying thresholding. Calculating the number of pixels remaining in the final thresholding images can be treated as a hypothetical method for indicating the volume of reconstructed object. Figure 15, which shows the number of voxels remaining in final reconstructed images versus depth, indicates that the volume of samples being reconstructed by isotropic and anisotropic TV are approximately unaffected by increasing depth. Moreover, the reconstructed volume and cross-section size of the sample and can be approximately estimated from the reconstructed images shown in Figure 12. Table 5 and Table 5 explicitly list the estimated volume/ cross-section size of the object and the accuracy of volume/shape reconstruction.

Overall, isotropic TV and anisotropic TV can provide better volume and shape reconstruction performance than Tikhonov regularization in depth detection. However, isotropic and anisotropic TV presented similar performance, which may be explained by the fact that isotropic TV performed well for these data. While anisotropic TV can regularize differently along the depth direction, maybe a stronger prior may be needed to recover the loss of sensitivity with depth. In future work, we may consider machine learning, which has been recently proposed for learning inverse problems and seems to be a good candidate to model and correct for depth in planar MIT(Deans et al., 2018).

Figure 15 Volume of reconstructed objects against depth

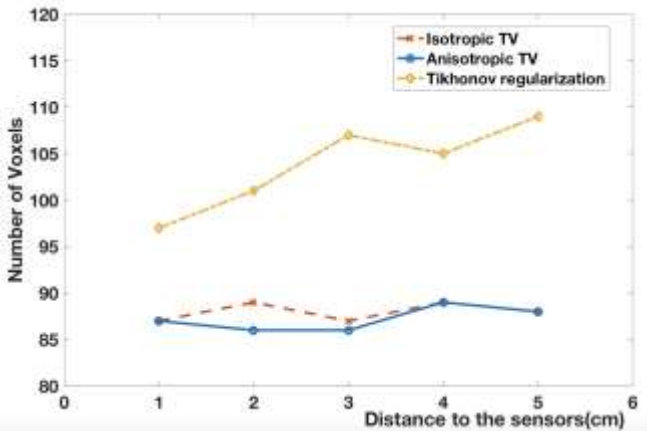

Table 5 Estimated experimental volume of the samples and volume reconstruction accuracies

Depth (cm)	Estimated Volume	Isotropic TV (cm^3)	Anisotropic TV (cm^3)	Tikhonov (cm^3)

1	Actual Volume $62.85cm^3$	87	87	97
2		89	86	101
3		87	86	107
4		89	89	105
5		88	88	109
Average accuracy		59.7%	61.3%	23.9%

Table 6 Estimated experimental cross-section size of the samples and shape reconstruction accuracies

Depth (cm)	Estimated Size	Isotropic TV (cm^2)	Anisotropic TV (cm^2)	Tikhonov (cm^2)
1	Actual Size $12.57cm^2$	16	16	14
2		19	16	22
3		19	17	21
4		16	16	22
5		17	16	20
Average accuracy		61.6%	71.1%	42.5%

5. Conclusion

The capability of planar sensor array MIT system has been investigated using experimental data. Reconstructed images obtained by isotropic and anisotropic TV indicate the position and shape of the samples precisely, which certify the capability of planar sensor array MIT system for depth detection and verify that isotropic and anisotropic TV algorithm can produce higher quality reconstructed images compared to Tikhonov regularization. Even if detectability works only for limited depth, it validated the potential application of planar MIT system for subsurface imaging. The results of enhanced depth detection shown in this study opens up further new applications for planar array MIT.

6. Acknowledgements

We would like to thank anonymous referees for their careful reviewing the article.

REFERENCES

ABASCAL, J. F., ABELLA, M., MARINETTO, E., PASCAU, J. & DESCO, M. 2016. A Novel Prior- and Motion-Based Compressed Sensing Method for Small-Animal Respiratory Gated CT. *PloS one,* 11**,** e0149841.

ABASCAL, J. J., CHAMORRO‐SERVENT, J., AGUIRRE, J., ARRIDGE, S., CORREIA, T., RIPOLL, J., VAQUERO, J. J. & DESCO, M. 2011. Fluorescence diffuse optical tomography using the split Bregman method. *Medical physics,* 38**,** 6275-6284.

BÍRÓ, O. 1999. Edge element formulations of eddy current problems. *Computer methods in applied mechanics and engineering,* 169**,** 391-405.

BIRO, O. & PREIS, K. 1989. On the use of the magnetic vector potential in the finite-element analysis of three-dimensional eddy currents. *IEEE Transactions on magnetics,* 25**,** 3145-3159.

BURGER, M., MENNUCCI, A. C., OSHER, S. & RUMPF, M. 2013. *Level Set and PDE Based Reconstruction Methods in Imaging: Cetraro, Italy 2008, Editors: Martin Burger, Stanley Osher*, Springer.

CHEN, Z., JIN, X., LI, L. & WANG, G. 2013. A limited-angle CT reconstruction method based on anisotropic TV minimization. *Physics in medicine and biology,* 58**,** 2119.

CORREIA, T., AGUIRRE, J., SISNIEGA, A., CHAMORRO-SERVENT, J., ABASCAL, J., VAQUERO, J. J., DESCO, M., KOLEHMAINEN, V. & ARRIDGE, S. 2011. Split operator method for fluorescence diffuse optical tomography using anisotropic diffusion regularisation with prior anatomical information. *Biomedical optics express,* 2**,** 2632-2648.

DARRER, B. J., WATSON, J. C., BARTLETT, P. & RENZONI, F. 2015. Magnetic imaging: a new tool for UK national nuclear security. *Scientific reports,* 5.

DEANS, C., GRIFFIN, L. D., MARMUGI, L. & RENZONI, F. 2018. Machine learning based localization and classification with atomic magnetometers. *Physical Review Letters,* 120**,** 033204.

ESEDOḠLU, S. & OSHER, S. J. 2004. Decomposition of images by the anisotropic Rudin‐Osher‐Fatemi model. *Communications on pure and applied mathematics,* 57**,** 1609-1626.

GOLDFINE, N. Near surface material property profiling for determination of SCC susceptibility. 4th EPRI Balance-of-Plant Heat Exchanger NDE Symposium, WY, June 10-12, 1996, 1996.

GOLDSTEIN, T. & OSHER, S. 2009. The split Bregman method for L1-regularized problems. *SIAM journal on imaging sciences,* 2**,** 323-343.

LI, F., ABASCAL, J. F., DESCO, M. & SOLEIMANI, M.

2017. Total variation regularization with split Bregman-based method in magnetic induction tomography using experimental data. *IEEE Sensors Journal,* 17**,** 976-985.

LOU, Y., ZENG, T., OSHER, S. & XIN, J. 2015. A weighted difference of anisotropic and isotropic total variation model for image processing. *SIAM Journal on Imaging Sciences,* 8**,** 1798-1823.

MA, L., WEI, H.-Y. & SOLEIMANI, M. 2013. Planar magnetic induction tomography for 3D near subsurface imaging. *Progress In Electromagnetics Research,* 138**,** 65-82.

MA, X., PEYTON, A. J., BINNS, R. & HIGSON, S. R. 2005. Electromagnetic techniques for imaging the cross-section distribution of molten steel flow in the continuous casting nozzle. *IEEE Sensors Journal,* 5**,** 224-232.

MERWA, R., HOLLAUS, K., BRUNNER, P. & SCHARFETTER, H. 2005. Solution of the inverse problem of magnetic induction tomography (MIT). *Physiological Measurement,* 26**,** S241.

MUKHOPADHYAY, S., YAMADA, S. & IWAHARA, M. 2001. Inspection of electroplated materials--performance comparison with planar meander and mesh type magnetic sensor. *International Journal of Applied Electromagnetics and Mechanics,* 15**,** 323-329.

OSHER, S., BURGER, M., GOLDFARB, D., XU, J. & YIN, W. 2005. An iterative regularization method for total variation-based image restoration. *Multiscale Modeling & Simulation,* 4**,** 460-489.

PARK, G. S. & KIM, D. S. 2005. Development of a magnetic inductance tomography system. *IEEE transactions on magnetics,* 41**,** 1932-1935.

RAMLI, S. & PEYTON, A. Feasibility study of planar-array electromagnetic inductance tomography (EMT). 1st World Congress on Industrial Process Tomography, 1999. 14-17.

RUDIN, L. I., OSHER, S. & FATEMI, E. 1992. Nonlinear total variation based noise removal algorithms. *Physica D: Nonlinear Phenomena,* 60**,** 259-268.

SOLEIMANI, M., LIONHEART, W. R., PEYTON, A. J., MA, X. & HIGSON, S. R. 2006. A three-dimensional inverse finite-element method applied to experimental eddy-current imaging data. *IEEE Transactions on Magnetics,* 42**,** 1560-1567.

LIONHEART, W. R., SOLEIMANI, M., PEYTON, A.J. 2003. Sensitivity Analysis of 3D Magnetic Induction Tomography (MIT). *3rd World Congress on Industrial Process Tomography.* Banff, Canada.

WANG, J., MA, J., HAN, B. & LI, Q. 2012. Split Bregman iterative algorithm for sparse reconstruction of electrical impedance tomography. *Signal Processing,* 92**,** 2952-2961.

WEI, H.-Y. & SOLEIMANI, M. 2012. A magnetic induction tomography system for prospective industrial processing applications. *Chinese Journal of Chemical Engineering,* 20**,** 406-410.

WERLBERGER, M., TROBIN, W., POCK, T., WEDEL, A., CREMERS, D. & BISCHOF, H. Anisotropic Huber-L1 Optical Flow. BMVC, 2009. 3.

YIN, W. & PEYTON, A. 2006. A planar EMT system for the detection of faults on thin metallic plates. *Measurement Science and Technology,* 17**,** 2130.